arXiv:nucl-ex/0501014v2 14 Feb 2006

Light-ion production in the interaction of 96 MeV neutrons with oxygen

U. Tippawan[1,2], S. Pomp[1]*, A. Ataç[1], B. Bergenwall[1,4], J. Blomgren[1], S. Dangtip[1], A. Hildebrand[1], C. Johansson[1], J. Klug[1], P. Mermod[1], L. Nilsson[1,3], M. Österlund[1], N. Olsson[1,5], A.V. Prokofiev[3], P. Nadel-Turonski[4], V. Corcalciuc[6], and A. J. Koning[7]

[1] *Department of Neutron Research, Uppsala University, Sweden*

[2] *Fast Neutron Research Facility, Chiang Mai University, Thailand*

[3] *The Svedberg Laboratory, Uppsala University, Sweden*

[4] *Department of Radiation Sciences, Uppsala University, Sweden*

[5] *Swedish Defence Research Agency, Stockholm, Sweden*

[6] *Institute of Atomic Physics, Heavy Ion Department, Bucharest, Romania*

[7] *Nuclear Research and Consultancy Group, Petten, The Netherlands*

Abstract

Double-differential cross sections for light-ion (p, d, t, ^{3}He and α) production in oxygen induced by 96 MeV neutrons are reported. Energy spectra are measured at eight laboratory angles from 20° to 160° in steps of 20°. Procedures for data taking and data reduction are presented. Deduced energy-differential and production cross sections are reported. Experimental cross sections are compared to theoretical reaction model calculations and experimental data at lower neutron energies in the literature. The measured proton data agree reasonably well with the results of the model calculations, whereas the agreement for the other particles is less convincing. The measured production cross sections for protons, deuterons, tritons and alpha particles support the

*Corresponding author, Tel. +46 18 471 6850, Fax. +46 18 471 3853, E-mail: stephan.pomp@tsl.uu.se

trends suggested by data at lower energies.
PACS numbers: 24.10.-i, 25.40.-h, 25.40.Hs, 25.40.Kv, 28.20.-v

1 Introduction

Fast-nucleon induced reactions provide useful means to investigate nuclear structure, to characterize reaction mechanisms and to impose stringent constraints on nuclear model calculations. Although oxygen is a light nucleus with doubly closed shells, it can be expected that many statistical assumptions hold for nucleon-induced reactions at several tens of MeV, because the level density at high excitation energies is sufficiently high that shell effects and other nuclear structure signatures are washed out. Light nuclei also have low Coulomb barrier, implying that the suppression of charged-particle emission is weak. Therefore, nuclear reaction models for equilibrium and pre-equilibrium decay can be tested and benchmarked. Experimental data on reactions in oxygen in the literature at incident neutron energies of 27, 40, and 60 MeV [1, 2] and between 25 and 65 MeV [3, 4, 5] offer possibilities to test the predictions of reaction models.

In recent years, an increasing number of applications involving fast neutrons have been developed or are under consideration, e.g., radiation treatment of cancer [6, 7, 8], neutron dosimetry at commercial aircraft altitudes [9], soft-error effects in computer memories [10, 11], accelerator-driven transmutation of nuclear waste and energy production [12, 13], and determination of the response of neutron detectors [14]. Data on light-ion production in light nuclei such as carbon, nitrogen and oxygen are particularly important in calculations of dose distributions in human tissue for radiation therapy at neutron beams, and for dosimetry of high energy neutrons produced by high-energy cosmic radiation interacting with nuclei (nitrogen and oxygen) in the atmosphere [9, 15]. When studying neutron dose effects in radiation therapy and at high altitude, it is especially important to consider oxygen, because it is the dominant element (65 % by weight) in average human tissue.

In this paper, we present experimental double-differential cross sections (inclusive yields) for protons, deuterons, tritons, ^{3}He and alpha particles produced by 96 MeV neutrons incident on oxygen. The measurements have been performed at the cyclotron of The Svedberg Laboratory (TSL), Uppsala, using the MEDLEY experimental setup [16]. Spectra have been measured at 8 laboratory angles, ranging from 20° to 160° in 20° steps. Extrapolation procedures are used to obtain coverage of the full angular range, and consequently energy-differential and production cross sections are deduced, the latter by integrating over energy and angle. The experimental data are com-

pared to results of calculations with nuclear reaction codes and to existing experimental data at lower incident neutron energies.

The experimental methods are briefly discussed in Sec. 2 and data reduction and correction procedures are presented in Sec. 3. The theoretical framework is summarized in Sec. 4. In Sec. 5, the experimental results are reported and compared with theoretical and previous experimental data. Conclusions and an outlook are given in Sec. 6.

2 Experimental methods

The experimental setup, procedures for data reduction and corrections have been described in detail recently [17, 18] and therefore only brief summaries are given here.

The neutron beam facility at The Svedberg Laboratory (TSL) uses the ^{7}Li(p,n)^{7}Be reaction to produce a quasi-monoenergetic neutron beam [19]. The lithium target was 8 mm thick in the present experiment and enriched to 99.98 % in ^{7}Li. The 98.5±0.3 MeV protons from the cyclotron impinge on the lithium target, producing neutrons with a full-energy peak of 95.6±0.5 MeV with a width of 1.6 MeV (FWHM). With a beam intensity of 5 μA, the neutron flux in the full-energy peak is about $5{\cdot}10^{4}$ neutrons/(s·cm^{2}) at the target location. The collimated neutron beam has a diameter of 80 mm at the location of the target, where it is monitored by a thin film breakdown counter (TFBC) [20]. Relative monitoring was obtained by charge integration of the proton beam in a Faraday cup located in the proton beam dump. The two beam monitor readings were in agreement during the measurements.

The charged particles are detected by the MEDLEY setup [16]. It consists of eight three-element telescopes mounted inside a 100 cm diameter evacuated reaction chamber. Each telescope consists of two fully depleted ΔE silicon surface barrier detectors and a CsI(Tl) crystal. The thickness of the first ΔE detector (ΔE_1) is either 50 or 60 μm, while the second one (ΔE_2) is either 400 or 500 μm. They are all 23.9 mm in diameter (nominal). The cylindrical CsI(Tl) crystal, 50 mm long and 40 mm in diameter, serves as the E detector.

A 22 mm diameter 500 μm thick (cylindrical) disk of SiO_2 is used as the oxygen target. For the subtraction of the silicon contribution, measurements using a silicon wafer having a 32·32 mm^{2} quadratic shape and a thickness of 303 μm are performed.

For absolute cross section normalization, a 25 mm diameter and 1.0 mm thick polyethylene $(CH_2)_n$ target is used. The np cross section at 20° laboratory angle provides the reference cross section [21]. Instrumental background

is measured by removing the target from the neutron beam. It is dominated by protons produced by neutron beam interactions with the beam tube and reaction chamber material, especially at the entrance and exit of the reaction chamber and in the telescope housings. Therefore, the telescopes at 20° and 160° are most affected.

The time-of-flight (TOF) obtained from the radio frequency of the cyclotron (stop signal for TDCs) and the timing signal from each of the eight telescopes (start signal) is registered for each charged-particle event. Typical count rates for target-in and target-out runs were 10 and 2 Hz, respectively. The dead time of the data acquisition system was typically $1-2$ % and never exceeded 10 %.

3 Data reduction procedures and corrections

The $\Delta E - E$ technique is used to identify light charged particles ranging from protons to lithium ions. Good separation of all particles is obtained over their entire energy range and particle identification is straightforward.

Energy calibration of all detectors is obtained from the data themselves [17, 18]. Events in the $\Delta E - E$ bands are fitted with respect to the energy deposited in the two silicon detectors. This energy is determined from the detector thicknesses and tabulated energy loss values in silicon [22]. The ΔE_1 detectors are further calibrated and checked using a 5.48 MeV alpha source. For the energy calibration of the CsI(Tl) detectors, two parameterizations of the light output versus energy of the detected particle [16, 17, 18] are used, one for hydrogen isotopes and another one for helium isotopes. Supplementary calibration points are provided by the H(n,p) reaction, as well as transitions to the ground state and low-lying states in the ^{12}C(n,d)^{11}B, ^{16}O(n,d)^{15}N and ^{28}Si(n,d)^{27}Al reactions. The energy of each particle is obtained by adding the energy deposited in each element of the telescope.

Low-energy charged particles are stopped in the ΔE_1 detector leading to a low-energy cutoff for particle identification of about 3 MeV for hydrogen isotopes and about 8 MeV for helium isotopes. The helium isotopes stopped in the ΔE_1 detector are nevertheless analyzed, and a remarkably low cutoff, about 4 MeV, can be achieved for the experimental alpha-particle spectra. These alpha-particle events could obviously not be separated from ^{3}He events in the same energy region, but the yield of ^{3}He is about a factor of 30 smaller than the alpha-particle yield in the region of 8 MeV, where the particle identification works properly. The assumption that the relative yield of ^{3}He is small is supported by the theoretical calculations in the evaporation peak region. In conclusion, the ^{3}He yield is within the statistical uncertainties of the

alpha-particle yield for alpha energies between 4 and 8 MeV. A consequence of this procedure is that the ^{3}He spectra have a low-energy cutoff of about 8 MeV.

Knowing the energy calibration and the flight distances, the flight time for each charged particle from target to detector can be calculated and subtracted from the measured total TOF. The resulting neutron TOF is used for selection of charged-particle events induced by neutrons in the main peak of the incident neutron spectrum.

Background events, collected in target-out runs and analyzed in the same way as target-in events, are subtracted from the corresponding target-in runs, with SiO_2 and silicon targets, after normalization to the same neutron fluence.

Due to the finite target thickness, corrections for energy loss and particle loss are applied to both targets individually. Details of the correction methods are described in Refs. [17, 23]. The cross sections for oxygen are obtained after subtraction of the silicon data from the SiO_2 data with proper normalization with respect to the number of silicon nuclei in the two targets.[1]

Even if a great majority of the neutrons appears in the narrow full-energy peak at 95.6 MeV, a significant fraction (about 13 %) belongs to a tail extending towards lower energies, remaining after the TOF cut, see Fig. 1. The average neutron energy with the tail neutrons included is 94.0 MeV. The particle spectra have not been unfolded with the neutron energy distribution, because it is anticipated that the energy variation of the cross sections is rather weak in the energy range of interest. Furthermore, the data set is called 96 MeV (95.6 MeV) data, because the peak of the distribution is quite dominant and any structure observed at the high-energy end of the ejectile spectra is due to the peak of the neutron energy dsitribution. The *np* cross section is, however, measured at the peak of the distribution (95.6 MeV) and corrected for the tail contribution. The correction to 94.0 MeV is performed using the known energy dependence of the *np* cross section.

Other corrections of the data are performed in analogy with the similar experiment dealing with silicon and described in detail in the corresponding publication [17]. The data and method for the efficiency correction of the CsI(Tl) detectors, reported in Ref. [19] and used in Ref. [17] and the present work, have recently [25] been corroborated by Monte Carlo calculations.

Absolute double-differential cross sections are obtained by normalizing the oxygen data to the number of recoil protons emerging from the CH_2

[1] In the process of extracting the oxygen data, the silicon data of Ref. [17] have been reanalyzed. In doing so, we have adapted some changes and also found two mistakes. See Ref. [24] in this issue.

target. After selection of events in the main neutron peak and proper subtraction of the target-out and ^{12}C(n,p) background contributions, the latter taken from a previous experiment, the cross section can be determined from the recoil proton peak, using *np* scattering data [21]. All data have been normalized using the *np* scattering peak in the 20° telescope.

4 Theoretical models

The present data have been compared with nuclear theory predictions, computed with the two nuclear reaction codes GNASH [26, 27] and TALYS [28]. While GNASH has been widely used during the last years, TALYS is a new code that has just been released in the public domain. The GNASH calculation is performed at a neutron energy of 100 MeV with parameters given in a recent evaluation for medical purposes [29] as described in Ref. [17]. Since oxygen is at the boundary of the mass range the TALYS code is aimed for, the code is described in some detail below.

Both GNASH and TALYS integrate direct, pre-equilibrium, and statistical nuclear reaction models into one calculation scheme and thereby give predictions for all the open reaction channels. Both codes use the Hauser-Feshbach model for sequential equilibrium decay and the exciton model for pre-equilibrium emission, though GNASH uses the one-component model, i.e. without isospin distinction of the excited nucleons, and TALYS uses the two-component model, see below. The angular distributions are obtained using the Kalbach systematics [30].

The purpose of TALYS is to simulate nuclear reactions that involve neutrons, photons, protons, deuterons, tritons, ^{3}He and alpha particles in the 1 keV – 200 MeV energy range. Predicted quantities include integrated, single- and double-differential cross sections, for both the continuum and discrete states, residue production and fission cross sections, gamma-ray production cross sections, etc. For the present work, single- and double-differential cross sections are of interest. To predict these, a calculation scheme is invoked which consists of a direct + pre-equilibrium reaction calculation followed by subsequent compound nucleus decay of all possible residual nuclides calculated by means of the Hauser-Feshbach model.

For the optical model potentials (OMP) of both neutrons and protons on ^{16}O up to 200 MeV, the global OMP of Ref. [31] was used. These potentials provide the necessary transmission coefficients for the statistical model calculations. Although the global neutron OMP has been validated for $A > 24$, at the high incident energy considered in this work, an adequate description of the basic scattering observables is expected, at least for the incident neutron

channel and the high energy inelastic scattering and charge-exchange leading to discrete states and the continuum. For the low-energy outgoing charged particles, the non-validated use of the global OMP may have larger consequences. Obviously, a system of a total of 17 nucleons can hardly be called statistical, and this short-coming may be reflected in the prediction of some of the observables that concern low emission energies. For complex particles, the optical potentials were directly derived from the nucleon potentials using the folding approach of Watanabe [32]. Finally, since applying the charged-particle OMP's for nuclides as light as ^{16}O may be physically dubious, we renormalize the obtained OMP transmission coefficients with the empirical non-elastic cross sections of Ref. [33].

The high-energy end of the ejectile spectra are described by pre-equilibrium emission, which takes place after the first stage of the reaction but long before statistical equilibrium of the compound nucleus is attained. It is imagined that the incident particle step-by-step creates more complex states in the compound system and gradually loses its memory of the initial energy and direction. The default pre-equilibrium model of TALYS is the two-component exciton model [34, 35]. A remark similar to that given above for the OMP applies: the two-component exciton model for nucleon reactions has been tested, rather successfully, against basically all available experimental nucleon spectra for $A > 24$ [34]. The current system $A = 17$, falls outside that mass range, and does not entirely qualify as a system that can be handled by fully statistical models such as the exciton model.

We recall the basic formula of Ref. [34] for the exciton model cross section,

$$\frac{d\sigma_k^{EM}}{dE_k} = \sigma^{CF} \sum_{p_\pi=p_\pi^0}^{p_\pi^{eq}} \sum_{p_\nu=p_\nu^0}^{p_\nu^{eq}} w_k(p_\pi, h_\pi, p_\nu, h_\nu, E_k) S_{pre}(p_\pi, h_\pi, p_\nu, h_\nu), \qquad (1)$$

where $p_\pi(p_\nu)$ is the proton (neutron) particle number and $h_\pi(h_\nu)$ the proton (neutron) hole number, σ^{CF} is the compound formation cross section, and S_{pre} is the time-integrated strength which determines how long the system remains in a certain exciton configuration. The initial proton and neutron particle numbers are denoted $p_\pi^0 = Z_p$ and $p_\nu^0 = N_p$ with $Z_p(N_p)$ being the proton (neutron) number of the projectile. In general, $h_\pi = p_\pi - p_\pi^0$ and $h_\nu = p_\nu - p_\nu^0$, so that the initial hole numbers are zero, i.e. $h_\pi^0 = h_\nu^0 = 0$, for primary pre-equilibrium emission. The pre-equilibrium part is calculated by Eq. (1), using $p_\pi^{eq} = p_\nu^{eq} = 6$, whereas the remainder of the reaction flux is distributed through the Hauser-Feshbach model. In addition, the never-come-back approximation is adopted.

The emission rate w_k for ejectile k with spin s_k is given by

$$w_k(p_\pi, h_\pi, p_\nu, h_\nu, E_k) = \frac{2s_k+1}{\pi^2\hbar^3}\mu_k E_k \sigma_{k,inv}(E_k)\frac{\omega(p_\pi - Z_k, h_\pi, p_\nu - N_k, h_\nu, E_x)}{\omega(p_\pi, h_\pi, p_\nu, h_\nu, E^{tot})}, \tag{2}$$

where $\sigma_{k,inv}(E_k)$ is the inverse reaction cross section as calculated from the optical model, and ω is the two-component particle-hole state density. The full reaction dynamics that leads to Eq. (1) is described in Refs. [34, 35]. We here restrict ourselves to the formulae given above since they contain the model- and parameter-dependent quantities. The expression for S_{pre} contains the adjustable transition matrix element M^2 for each possible transition between neutron-proton exciton configurations. A proton-neutron ratio of 1.6 for the squared internal transition matrix elements was adopted to give the best overall agreement with experiment, i.e., $M^2_{\pi\nu} = M^2_{\nu\pi} = 1.6M^2_{\pi\pi} = 1.6M^2_{\nu\nu} = 1.6M^2$. For ^{16}O, we use the following expression for the matrix element [34],

$$M^2 = \frac{0.6}{A^3}\left[6.8 + \frac{4.2\times10^5}{(\frac{E^{\rm tot}}{n}+10.7)^3}\right], \tag{3}$$

where n is the exciton number. Partial level density parameters $g_\pi = Z/17$ and $g_\nu = N/17$ were used in the equidistant spacing model for the partial level densities. Finally, an effective surface interaction well depth $V = 12$ MeV [34] was used.

At incident energies above several tens of MeV, the residual nuclides formed after binary emission may have so large excitation energy that the presence of additional fast particles inside the nucleus becomes possible. The latter can be imagined as strongly excited particle-hole pairs resulting from the first binary interaction with the projectile. The residual system is then clearly non-equilibrated and the excited particle that is high in the continuum may, in addition to the first emitted particle, also be emitted on a short time scale. This so-called multiple pre-equilibrium emission forms an alternative theoretical picture of the intra-nuclear cascade process, whereby the exact location and momentum of the particles are not followed, but instead the total energy of the system and the number of particle-hole excitations (exciton number). In actual calculations, the particle-hole configuration of the residual nucleus after emission of the ejectile, is re-entered as initial condition in Eq. (1). When looping over all possible residual configurations, the multiple pre-equilibrium contribution is obtained. In TALYS, multiple pre-equilibrium emission is followed up to arbitrary order, though for 96 MeV only secondary pre-equilibrium emission is significant.

It is well-known that semi-classical models, such as the exciton model, have always had some problems to describe angular distributions (essentially

because it is based on a compound-like concept instead of a direct one). Therefore, as mentioned previously, the double-differential cross sections are obtained from the calculated energy spectra using the Kalbach systematics [30].

To account for the evaporation peaks in the charged-particle spectra, multiple compound emission was treated with the Hauser-Feshbach model. In this scheme, all reaction chains are followed until all emission channels are closed. The Ignatyuk model [36] has been adopted for the total level density to account for the damping of shell effects at high excitation energies.

For pre-equilibrium reactions involving deuterons, tritons, ^{3}He and alpha particles, a statistical contribution from the exciton model is automatically calculated with the formalism described above. It is, however, well known that for nuclear reactions involving projectiles and ejectiles with different particle numbers, mechanisms like stripping, pick-up and knock-out play an important role and these direct-like reactions to the continuum are not covered by the exciton model. Therefore, Kalbach has developed a phenomenological contribution for these mechanisms [37], which is included in TALYS. Among the advantages over the older method (which is included in GNASH) we mention here a better consideration of the available phase space through normalized particle-hole state densities and a better empirical determination of the pick-up, stripping, knock-out strength parameters, enabled by the more extensive experimental database that is now available. It has recently been shown (see Table I of Ref. [38]) that for medium and heavy nuclides this method gives a considerable improvement over the older methods. The latter seemed to consistently underpredict neutron-induced reaction cross sections involving pick-up of one or a few nucleons. In this paper, the two methods meet again, this time for the prediction of reactions on a light nucleus, and their performance will be compared in the next section.

5 Results and discussion

5.1 Experimental results

Double-differential cross sections of ^{16}O(n,xlcp) reactions, where lcp stands for light charged particle, at laboratory angles of 20°, 40°, 100° and 140° for protons, deuterons, tritons, ^{3}He and alpha particles are shown in Figs. $2-6$, respectively, all angles plotted with the same cross section scale for each emitted particle to facilitate comparison of magnitudes. The choice of energy bin width depends on the energy resolution in the experiment, the thick target correction and acceptable statistics in each energy bin. The error bars

in Figs. 2 − 6 represent statistical uncertainties only.

The overall relative statistical uncertainties of individual points in the double-differential energy spectra at 20° are typically 8 % for protons, 13 % for deuterons, 20 % for tritons, 15 % for ^{3}He and 12 % for alpha particles. As the angular distributions are forward-peaked, these values increase with angle. The systematic uncertainty contributions are due to thick target correction (1 − 20 %), collimator solid angle (1 − 5 %), beam monitoring (2 − 3 %), number of oxygen nuclei (0.1 %), CsI(Tl) intrinsic efficiency (1 %), particle identification (1 %) and dead time (< 0.1 %). The uncertainty in the absolute cross section is about 5 %, which is due to uncertainties in *np* scattering angle, contribution from the low-energy continuum of the ^{7}Li(p,n) spectrum to the *np* scattering proton peak (3 %), reference *np* cross sections (2 %) [21], statistics in the *np* scattering proton peak (2 %), carbon contribution (0.1 %) and number of hydrogen nuclei (0.1 %).

From Figs. 2− 6 it is obvious that the charged-particle emission at forward angles from 96 MeV neutron irradiation of oxygen is dominated by proton, deuteron and alpha particle channels. The yield of deuterons is about a factor of 3 lower than for protons and the spectra of the two other particle types studied in this work (tritons and ^{3}He) are more than an order of magnitude weaker. All the spectra have more or less pronounced peaks at low energies (below 10 − 15 MeV), the angular distributions of which are not too far from isotropy except for alpha particles, where the yield at backward angles is about four times weaker than at 20°. The low-energy peak is not fully observed in the ^{3}He spectra due to the 8 MeV low-energy cutoff discussed in Sec. 3.

All the particle spectra at forward angles show relatively large yields at medium-to-high energies. The emission of high-energy particles is strongly forward-peaked and hardly visible in the backward hemisphere. It is a sign of particle emission before statistical equilibrium has been reached in the reaction process. In addition to this broad distribution of emitted particles, the deuteron spectra at forward angles show narrow peaks corresponding to transitions to the ground state and low-lying states in the final nucleus, ^{15}N. These transitions are most likely due to pick-up of weakly bound protons in the target nucleus, ^{16}O. A similar but less pronounced effect is observed in the proton spectra at forward angles. The structure observed in this case is due to transitions to Gamow-Teller states and other low-lying states with considerable single-particle strength [1].

5.2 Comparison with theoretical model calculations

In Figs. 2− 6 the experimental results are presented together with theoretical model calculations. The GNASH calculations of Ref. [29] have been done for protons, deuterons and alpha particles, whereas the TALYS calculations discussed in Sec. 4 have been performed for all five particle types. The TALYS calculations include a transformation of the calculated cross sections to the lab system. Also in the GNASH code a similar transformation from the c.m. to the lab system is performed using the kinematics of one-particle emission. Differences between data given in the lab and c.m. systems are particularly significant in this case, because oxygen is such a light nucleus.

Fig. 2 shows the comparison between the double-differential (n,px) experimental spectra and the calculations based on the TALYS and GNASH models. For protons above 25 MeV, both calculations give a reasonably good description of the spectra, although the calculated 20° cross sections, in particular the TALYS ones, fall below the experimental data. The low-energy statistical peak below 15 MeV in the spectra is considerably overpredicted by the two codes. The overestimate is particularly strong at backward angles for TALYS and at forward angles for GNASH.

The situation is quite different for the deuteron spectra (Fig. 3). None of the calculations do account very well for the data, although the GNASH code gives a reasonable description of the angular dependence of the cross section. For the TALYS code deviations between data and calculations of a factor of two or more are present. At forward angles the high-energy part is strongly overestimated, in particular by the TALYS code, indicating problems in the hole-strength treatment. It is obvious, however, that efforts have been spent in these calculations to include individual hole-state strengths. Such strengths are not included in the GNASH calculations, but in spite of this the average behavior of the cross section at high energies is in fair agreement with the data. Like for the proton spectra, the statistical peak is overpredicted by the TALYS calculations essentially at all angles, whereas the GNASH calculations seem to do a slightly better job in this case.

For tritons (Fig. 4), the TALYS calculation gives a fairly good description of the experimental data, except that it fails to account for an intensity bump around 15 MeV observed at forward angles.

The general trends of the forward-angle ^{3}He data (Fig. 5) are reasonably well described in the TALYS calculations although the cross sections are underestimated by a large factor. At backward angles the yield is very small and it is difficult to make quantitative comparisons.

The overall shapes of the alpha particle spectra (Fig. 6) are reasonably well described by the two models. The GNASH calculations, however, over-

predict the cross sections at forward angles and underpredict them at large angles, whereas the TALYS calculations do the opposite, i.e., underpredict at small angles and overpredict at large angles.

The ability of the models to account for the low-energy peak caused by evaporation processes (and for α particles also 3α breakup of ^{12}C) is not impressive. In general, the models tend to overpredict the cross sections. It should, however, be kept in mind that the peak maximum is close to (for ^{3}He below) the low-energy cutoff, which complicates the comparison. Another complication in this context is that the GNASH cross sections although given in the lab system, are calculated using the kinematics of one-particle emission [26, 27] for the c.m.-to-lab transformation, which obviously is an approximation.

Experimental angular distributions at low, medium and high ejectile energies are shown in Figs. 7 − 11 for protons, deuterons, tritons, ^{3}He and alpha particles, respectively. The angular distributions are fitted by a simple two parameter function, $a\exp(b\cos\theta)$ [30]. The data are compared with angular distributions calculated on the basis of the GNASH and TALYS models. In general, the TALYS model gives a weaker angular dependence than the data, whereas the GNASH model, although being closer to the data, tends to give a slightly steeper angular variation.

A conspicuous deviation from the experimental angular distribution is seen for the TALYS prediction at the lowest outgoing energies, e. g. at $8-12$ MeV in Fig. 7. We think this is attributed to wrong partial spectrum contributions to the total spectrum. The slightly forward-peaked angular distribution suggests that the spectrum at these emission energies is not as compound-dominated as the TALYS calculation suggests. Instead secondary, and even tertiary, pre-equilibrium emission may not be negligible even in the evaporation peak. Multiple pre-equilibrium emission is taken into account in TALYS but only contributes at somewhat higher emission energies. A way to make multiple pre-equilibrium (processes) relatively more important is to reduce the compound nucleus emission contribution, but we find that the predicted evaporation peak is rather insensitive to parameter variations. Hence, this is an open problem for TALYS, which apparently has been solved for the GNASH calculation.

5.3 Integrated spectra

For each energy bin of the light-ion spectra, the experimental angular distribution is fitted by a simple two-parameter function, $a\exp(b\cos\theta)$ [30], as exemplified in the previous subsection (Figs. 7 − 11). This allows extrapolation of double-differential cross sections to very forward and very backward

angles. In this way coverage of the full angular range is obtained. By integration of the angular distribution, energy-differential cross sections ($d\sigma/dE$) are obtained for each ejectile. These are shown in Fig. 12 together with theoretical calculations. For all ejectiles both calculations give a fair description of the energy dependence. Both calculations are in good agreement with the proton experimental data over the whole energy range, although the calculation for (n,p) reactions to discrete states is underestimating the data. A study of the spectroscopic strengths for these states would be welcome. Concerning the deuteron spectra, the GNASH calculations are in good agreement with the data, whereas the TALYS code gives cross sections a factor of two or more larger than the experimental ones at energies above 30 MeV. In the case of alpha particles, the GNASH calculation tends to overpredict the high-energy part of the spectrum, and the TALYS calculations fall below the data above an alpha particle energy of 25 MeV. The energy dependence of the triton and ^{3}He spectra are well described by the TALYS code, but in both cases the calculation falls below the data above about 20 MeV.

The production cross sections are deduced by integration of the energy-differential spectra (see Table 1). To be compared with the calculated cross sections, the experimental values in Table 1 have to be corrected for the undetected particles below the low-energy cutoff. This is particularly important for ^{3}He because of the high cutoff energy. The corrections obtained with TALYS seem to be too small in some cases, in particular for the (n,xα) production cross section. This is illustrated in Fig. 12, bottom panel, where the TALYS curve falls well below the experimental $d\sigma/dE$ data in the 4–7 MeV region.

The proton, deuteron, triton, and alpha particle production cross sections are compared with previous data at lower energies [5] in Fig. 13. There seems to be general agreement between the trends of the previous data and the present data points. The curves in this figure are based on a GNASH calculation [29].

6 Conclusions and outlook

In the present paper, we report an experimental data set on light-ion production in oxygen induced by 96 MeV neutrons. Experimental double-differential cross sections ($d^2\sigma/d\Omega dE$) are measured at eight angles between 20° and 160°. Energy-differential ($d\sigma/dE$) and production cross sections are obtained for the five types of outgoing particles. Theoretical calculations based on nuclear reaction codes including direct, pre-equilibrium and statistical models give generally a good account of the magnitude of the experimental cross sec-

tions. For proton emission, the shape of the spectra for the double-differential and energy-differential cross sections are well described. The calculated and the experimental alpha-particle spectra are also in fair agreement with the exception of the high energy part, where the GNASH model predicts higher yield and the TALYS model lower yield than experimentally observed. For the proton evaporation peak, the global TALYS calculation overestimates the data. A future activity should be an adjustment of the responsible OMP and level density parameters (as was done in the case of GNASH) instead of relying on a full global prediction. For the other complex ejectiles (deuteron, triton and ^{3}He) there are important differences between theory and experiment in what concerns the shape of the spectra at various angles. We think this is due to the use of statistical models such as the Hauser-Feshbach model and the pre-equilibrium exciton model in mass ranges where these models become suspect, and the absence of a break-up model in the theoretical analysis. Apart from the aforementioned break-up model, predictions of emission of alpha particles may be particularly sensitive to a correct knock-out model and the use of adequate complex particle optical model potentials. Stripping and knock-out models, level densities, optical model and omission of break-up reactions may all add up to problems for something as light as oxygen. This needs to be studied in much more detail. Finally, the magnitude of the angle-integrated cross sections is reasonably well accounted for.

For the further development of the field, data at even higher energies are requested. The results suggest that the MEDLEY facility, which was used in the present work, should be upgraded to work also at 180 MeV, i.e., the maximum energy of the TSL neutron beam facility. At present, a new neutron beam facility is under commissioning at TSL [39], covering the same energy range, but with a projected intensity increase of a factor five. This will facilitate measurements at energies higher than in the present work.

Acknowledgments

This work was supported by the Swedish Natural Science Research Council, the Swedish Nuclear Fuel and Waste Management Company, the Swedish Nuclear Power Inspectorate, Ringhals AB, the Swedish Defence Research Agency, and the Swedish International Development Authority. The authors wish to thank the The Svedberg Laboratory for excellent support. One of the authors (U.T.) wishes to express his gratitude to the Thai Ministry of University Affairs and to the International Program in the Physical Sciences at Uppsala University.

References

[1] G. A. Needham, F. P. Brady, D. H. Fitzgerald, J. L. Romero, J. L. Ullmann, J. W. Watson, C. I. Zanelli, N. S. P. King, and G. R. Satchler, Nucl. Phys. **A385**, 349 (1982).

[2] T. S. Subramanian, J. L. Romero, F. P. Brady, D. H. Fitzgerald, R. Garrett, G. A. Needham, J. L. Ullmann, J. W. Watson, C. I. Zanelli, D. J. Brenner, and R. E. Prael, Phys. Rev. C **34**, 1580 (1986).

[3] S. Benck, I. Slypen, J.P. Meulders, and V. Corcalciuc, Eur. Phys. J. **3**, 149 (1998).

[4] S. Benck, I. Slypen, J.P. Meulders, and V. Corcalciuc, Eur. Phys. J. **3**, 159 (1998).

[5] S. Benck, I. Slypen, J.P. Meulders, and V. Corcalciuc, Phys. Med. Biol. **43**, 3427 (1998).

[6] R. Orecchia, A. Zurlo, A. Loasses, M. Krengli, G. Tosi, S. Zurrida, P. Zucali, and U. Veronesi, Eur. J. Cancer **34**, 459 (1998).

[7] D.L. Schwartz, J. Einck, J. Bellon, and G.E. Laramore, Int. J. Radiat. Oncol. Biol. Phys. **50**, 449 (2001).

[8] G.E. Laramore and T.W. Griffin, Int. J. Radiat. Oncol. Biol. Phys. **32**, 879 (1995).

[9] D.T. Bartlett, R. Grillmaier, W. Heinrich, L. Lindborg, D. O'Sullivan, H. Schraube, M. Silari, and L. Tommasino, Radiat. Res. Congress Proceedings **2**, 719 (2000). See also the Proceedings of the International Conference on Cosmic Radiation and Aircrew Exposure, Radiat. Prot. Dosim. **86(4)** (1999).

[10] Single-Event Upsets in Microelectronics, topical issue, eds. H.H.K. Tang and N. Olsson, Mat. Res. Soc. Bull. **28** (2003).

[11] M.B. Chadwick and E. Normand, IEEE Trans. Nucl. Sci. **46**, 1386 (1999).

[12] High and Intermediate energy Nuclear Data for Accelerator-driven Systems (HINDAS), European contract FIKW-CT-2000-00031, coord. J.P. Meulders.

[13] A. Koning, H. Beijers, J. Benlliure, O. Bersillon, J. Blomgren, J. Cugnon, M. Duijvestijn, Ph. Eudes, D. Filges, F. Haddad, S. Hilaire, C. Lebrun, F.-R. Lecolley, S. Leray, J.-P. Meulders, R. Michel, R.-D. Neef, R. Nolte, N. Olsson, E. Ostendorf, E. Ramström, K.-H. Schmidt, H. Schuhmacher, I. Slypen, H.-A. Synal, and R. Weinreich, J. Nucl. Sci. Tech., Suppl. **2**, 1161 (2002).

[14] R.A. Cecil, B.D. Anderson, and R. Madey, Nucl. Instr. Meth. **161**, 439 (1979).

[15] J. Blomgren and N. Olsson, Radiat. Prot. Dosim. **103(4)**, 293 (2003).

[16] S. Dangtip, A. Ataç, B. Bergenwall, J. Blomgren, K. Elmgren, C. Johansson, J. Klug, N. Olsson, G. Alm Carlsson, J. Söderberg, O. Jonsson, L. Nilsson, P.-U. Renberg, P. Nadel-Turonski, C. Le Brun, F.R. Lecolley, J.F. Lecolley, C. Varignon, Ph. Eudes, F. Haddad, M. Kerveno, T. Kirchner, and C. Lebrun, Nucl. Instr. Meth. Phys. Res. A **452**, 484 (2000).

[17] U. Tippawan, S. Pomp, A. Ataç, B. Bergenwall, J. Blomgren, S. Dangtip, A. Hildebrand, C. Johansson, J. Klug, P. Mermod, L. Nilsson, M. Österlund, N. Olsson, K. Elmgren, O. Jonsson, A. V. Prokofiev, P.-U. Renberg, P. Nadel-Turonski, V. Corcalciuc, Y. Watanabe, and A. J. Koning, Phys. Rev. C **69**, 064609 (2004).

[18] U. Tippawan, Doctoral thesis, Chiang Mai University (2004) (unpublished).

[19] J. Klug, J. Blomgren, A. Ataç, B. Bergenwall, S. Dangtip, K. Elmgren, C. Johansson, N. Olsson, S. Pomp, A.V. Prokofiev, J. Rahm, U. Tippawan, O. Jonsson, L. Nilsson, P.-U. Renberg, P. Nadel-Turonski, A. Ringbom, A. Oberstedt, F. Tovesson, V. Blideanu, C. Le Brun, J.F. Lecolley, F.R. Lecolley, M. Louvel, N. Marie, C. Schweitzer, C. Varignon, Ph. Eudes, F. Haddad, M. Kerveno, T. Kirchner, C. Lebrun, L. Stuttgé, I. Slypen, A. Smirnov, R. Michel, S. Neumann, and U. Herpers, Nucl. Instr. Meth. Phys. Res. A **489**, 282 (2002).

[20] A.N. Smirnov, V.P. Eismont, and A.V. Prokofiev, Rad. Meas. **25**, 151 (1995).

[21] J. Rahm, J. Blomgren, H. Condé, S. Dangtip, K. Elmgren, N. Olsson, T. Rönnqvist, R. Zorro, O. Jonsson, L. Nilsson, P.-U. Renberg, A. Ringbom, G. Tibell, S.Y. van der Werf, T.E.O. Ericson, and B. Loiseau, Phys. Rev. C **63**, 044001 (2001).

[22] J.F. Ziegler, TRIM Code, version 95.4, IBM-Research, 1995.

[23] S. Pomp, Internal note (unpublished).

[24] U. Tippawan, S. Pomp, A. Ataç, B. Bergenwall, J. Blomgren, S. Dangtip, A. Hildebrand, C. Johansson, J. Klug, P. Mermod, L. Nilsson, M. Österlund, N. Olsson, K. Elmgren, O. Jonsson, A.V. Prokofiev, P.-U. Renberg, P. Nadel-Turonski, V. Corcalciuc, Y. Watanabe, A. Koning, Phys. Rev. C **XX**, xxxxxx(E) (2006).

[25] V. Blideanu, F.R. Lecolley, J.F. Lecolley, T. Lefort, N. Marie, A. Ataç, G. Ban, B. Bergenwall, J. Blomgren, S. Dangtip, K. Elmgren, Ph. Eudes, Y. Foucher, A. Guertin, F. Haddad, A. Hildebrand, C. Johansson, O. Jonsson, M. Kerveno, T. Kirchner, J. Klug, Ch. Le Brun, C. Lebrun, M. Louvel, P. Nadel-Turonski, L. Nilsson, N. Olsson, S. Pomp, A.V. Prokofiev, P.-U. Renberg, G. Rivière, I. Slypen, L. Stuttgé, U. Tippawan, and M. Österlund, Phys. Rev. C **70**, 014607 (2004).

[26] P.G. Young, E.D. Arthur, and M.B. Chadwick, Los Alamos National Laboratory Report No LA-12343-MS (1992), GNASH-FKK version gn9cp0, PSR-0125.

[27] M.B. Chadwick, P.G. Young, R.E. MacFarlane, and A.J. Koning, Proc. of 2nd Int. Conf. Accelerator-Driven Transmutation Technologies and Applications, Kalmar, Sweden, 1996, edited by H. Condé (Gotab, Stockholm, Sweden, 1997), p. 483.

[28] A.J. Koning, S. Hilaire, and M.C. Duijvestijn, TALYS-0.64 User Manual, December 5, 2004, NRG Report 21297/04.62741/P FAI/AK/AK.

[29] ICRU Report **63**, International Commission on Radiation Units and Measurements, Bethesda, MD, March 2000.

[30] C. Kalbach, Phys. Rev. C **37**, 2350 (1988).

[31] A.J. Koning and J.P. Delaroche, Nucl. Phys. A **713**, 231 (2003).

[32] S. Watanabe, Nucl. Phys. **8**, 484 (1958).

[33] R.K. Tripathi, F.A. Cucinotta, and J.W. Wilson, Nucl. Instr. Meth. Phys. Res. B **117**, 347 (1996).

R.K. Tripathi, F.A. Cucinotta, and J.W. Wilson, NASA technical paper 3621, January 1997.

[34] A.J. Koning, and M.C. Duijvestijn, Nucl. Phys. **A744**, 15 (2004).

[35] C. Kalbach, Phys. Rev. C **33** , 818 (1986).

[36] A.V. Ignatyuk, G.N. Smirenkin, and A.S. Tishin, Sov. J. Nucl. Phys. **21**, 255 (1975).

[37] C. Kalbach, Users manual for PRECO-2000, Duke University (2001).

C. Kalbach, Phys. Rev. C **71**, 034606 (2005).

[38] M. Kerveno, F. Haddad, Ph. Eudes, T. Kirchner, C. Lebrun, I. Slypen, J. P. Meulders, C. Le Brun, F. R. Lecolley, J. F. Lecolley, M. Louvel, F. Lefèbvres, S. Hilaire, and A. J. Koning, Phys. Rev. C **66**, 014601 (2002).

[39] S. Pomp, A.V. Prokofiev, J. Blomgren, C. Ekström, O. Jonsson, D. Reistad, V. Ziemann, N. Haag, A. Hildebrand, L. Nilsson, B. Bergenwall, C. Johansson, P. Mermod, N. Olsson, M. Österlund, and U. Tippawan, The new Uppsala neutron beam facility, Proceedings of International Conference on Nuclear Data for Science and Technology, Santa F, NM, September 26 - October 1 2004, AIP Conference Proceedings No. 769 (Melville, New York, 2005), 780.

Figure captions

1. Neutron energy distribution with the time-of-flight criterion applied derived from *np* scattering data at an angle of 20 degrees. The peak (95.6 MeV), median (95.1 MeV) and average (94.0 MeV) are indicated by solid, dashed and dotted vertical lines, respectively.

2. Experimental double-differential cross sections (filled circles) of the O(n,px) reaction at 96 MeV at four laboratory angles. The curves indicate theoretical calculations based on GNASH (dotted) and TALYS (solid).

3. Experimental double-differential cross sections (filled circles) of the O(n,dx) reaction at 96 MeV at four laboratory angles. The curves indicate theoretical calculations based on GNASH (dotted) and TALYS (solid).

4. Experimental double-differential cross sections (filled circles) of the O(n,tx) reaction at 96 MeV at four laboratory angles. The curve indicates theoretical calculations based on TALYS.

5. Experimental double-differential cross sections (filled circles) of the O(n,^{3}Hex) reaction at 96 MeV at four laboratory angles. The curve indicates theoretical calculations based on TALYS.

6. Experimental double-differential cross sections (filled circles) of the O(n,αx) reaction at 96 MeV at four laboratory angles. The curves indicate theoretical calculations based on GNASH (dotted) and TALYS (solid).

7. Angular distributions of O(n,px) cross section at ejectile energies of 8 - 12 MeV (filled circles), 40 - 44 MeV (filled triangles) and 68 - 72 MeV (open squares). The dashed curves are fits to the data and the dotted and solid curves represent calculations based on the GNASH and TALYS models, respectively.

8. Same as Fig. 7 but for the O(n,dx) cross section.

9. Same as Fig. 7 but for the O(n,tx) cross section. No calculations based on the GNASH model are available for tritons.

10. Angular distributions of O(n,^{3}Hex) cross section at ejectile energies of 10 - 15 MeV (filled circles), 40 - 45 MeV (filled triangles) and 65 - 70

MeV (open squares). The dashed curves are fits to the data and the solid curves represent calculations based on the TALYS model.

11. Same as Fig. 10 but for the O(n,αx) cross section. The dotted curves represent calculations based on the GNASH model.

12. Experimental energy-differential cross sections (filled circles) for neutron-induced p, d, t, ^{3}He and α production at 96 MeV. The curves indicate theoretical calculations based on GNASH (dotted) and TALYS (solid).

13. Neutron-induced a) proton, b) deuteron, c) triton, and d) alpha particle production cross section as a function of neutron energy. The full circles are from the present work, whereas the open circles are from previous work [5]. The curves are based on a GNASH calculation. The data as well as the calculations correspond to cutoff energies of 6 MeV for protons and deuterons and 12 MeV for tritons and alpha particles. Note that the cutoff energies are different from those in Table 1.

Table 1: Experimental production cross sections for protons, deuterons, tritons, ^{3}He and alpha particles from the present work. The experimental data in the second column have been obtained with cutoff energies of 2.5, 3.0, 3.5, 8.0 and 4.0 MeV for p, d, t, ^{3}He and alpha particles, respectively. The third and forth columns show data corrected for these cutoffs, using the GNASH (Ref. [29]) and the TALYS calculations of the present work, respectively. Theoretical values resulting from GNASH and TALYS calculations are in the fifth and sixth columns, respectively.

σ_{prod}	Experiment	Experiment [cutoff corr.]		Theoretical calculation	
	(mb)	GNASH	TALYS	GNASH	TALYS
(n,px)	224±11	248	231	259.9	221.7
(n,dx)	72±4	80	73	73.4	131.3
(n,tx)	20±1	–	20	–	10.6
(n,^{3}Hex)	6.9±0.6	–	8.7	–	8.2
(n,αx)	132±7	218	132	224.7	88.4

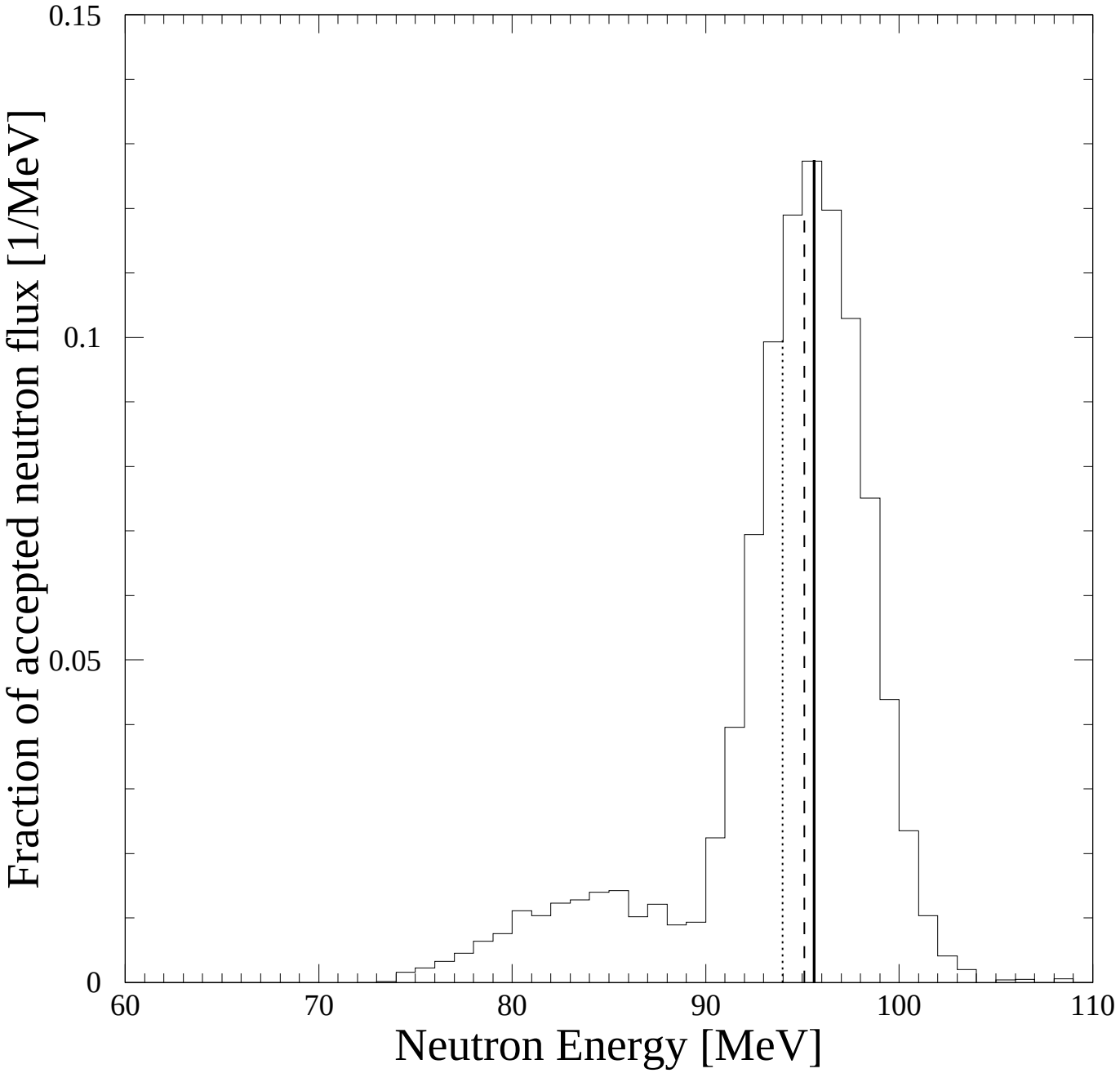
0.15
0.1
0.05
0
Fraction of accepted neutron flux [1/MeV]
60
70
80
90
100
110
Neutron Energy [MeV]

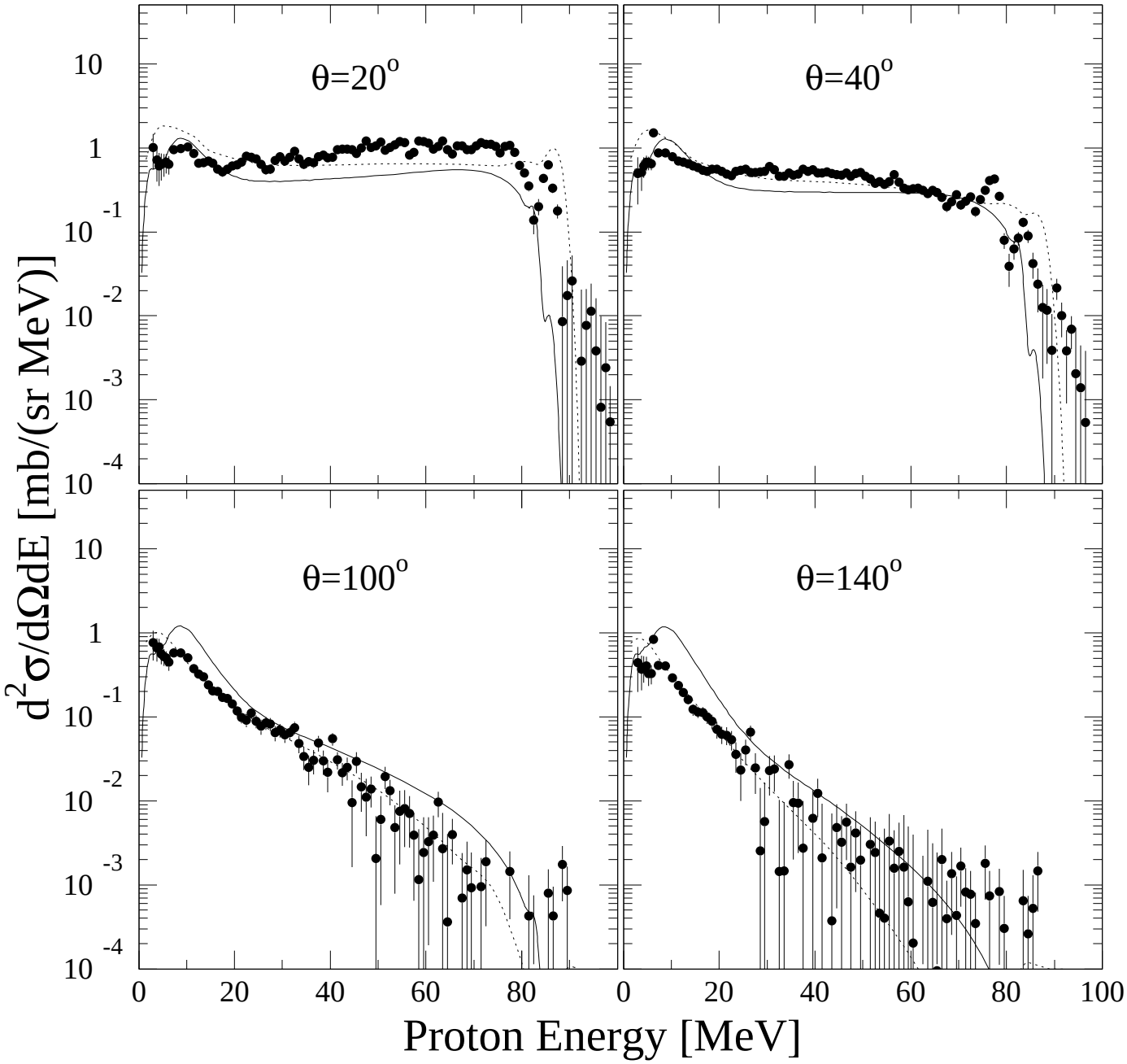
θ=20°
θ=40°
θ=100°
θ=140°
d²σ/dΩdE [mb/(sr MeV)]
Proton Energy [MeV]
10
1
10⁻¹
10⁻²
10⁻³
10⁻⁴
0
20
40
60
80
100

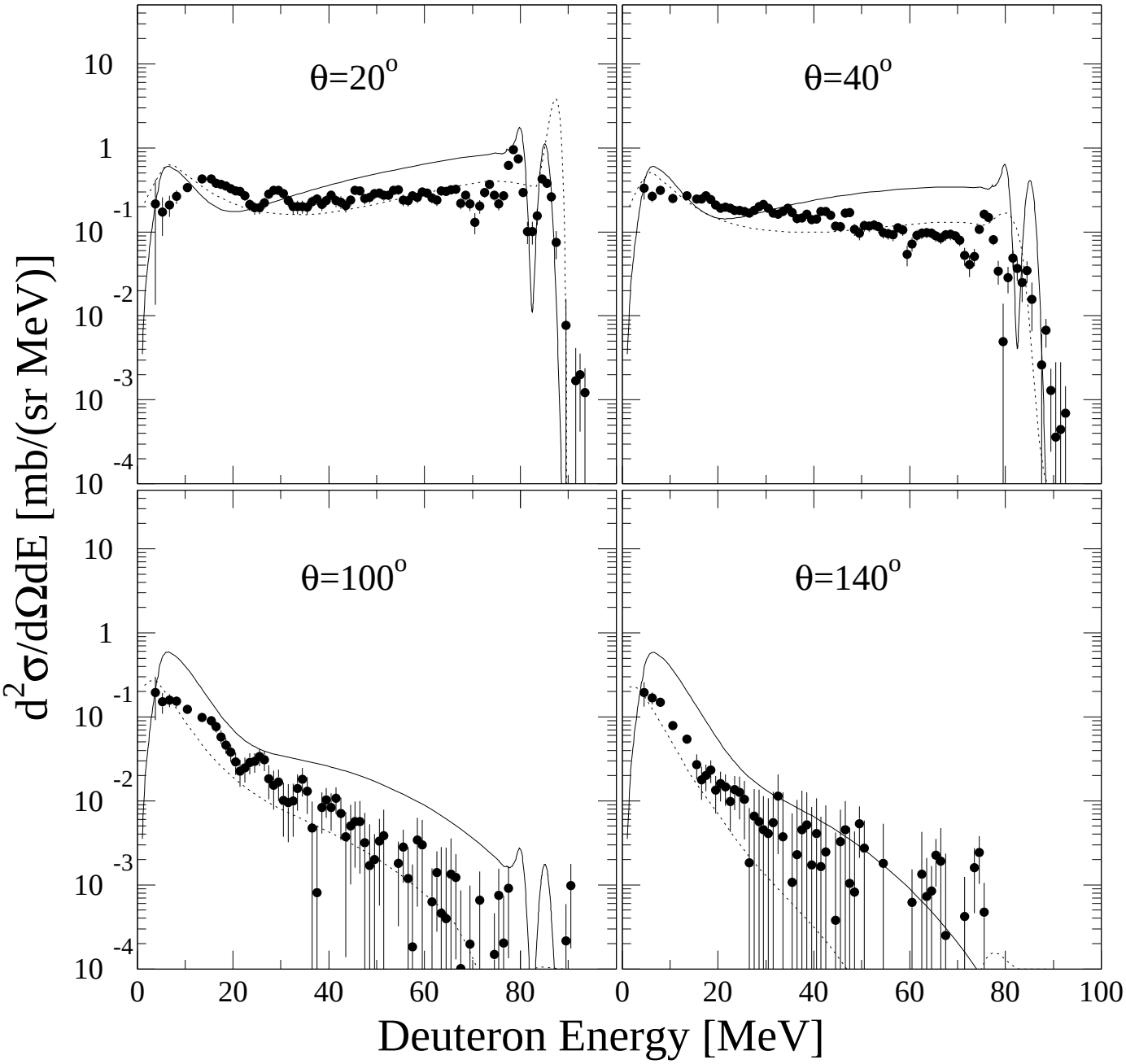
θ=20°
θ=40°
θ=100°
θ=140°
d²σ/dΩdE [mb/(sr MeV)]
Deuteron Energy [MeV]
10
1
10⁻¹
10⁻²
10⁻³
10⁻⁴
0
20
40
60
80
100

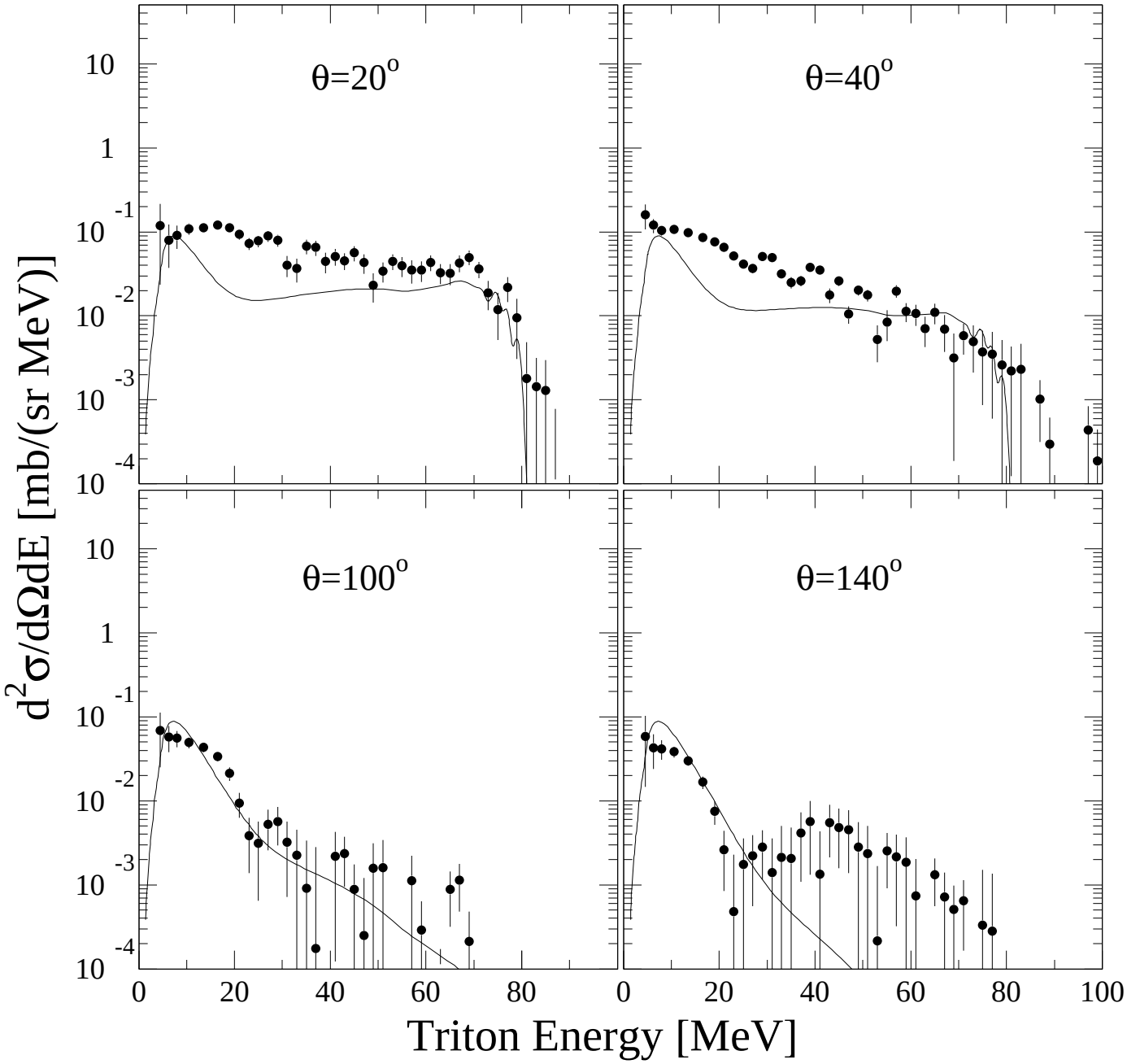
θ=20°
θ=40°
θ=100°
θ=140°
d²σ/dΩdE [mb/(sr MeV)]
Triton Energy [MeV]
10
1
10⁻¹
10⁻²
10⁻³
10⁻⁴
0
20
40
60
80
100

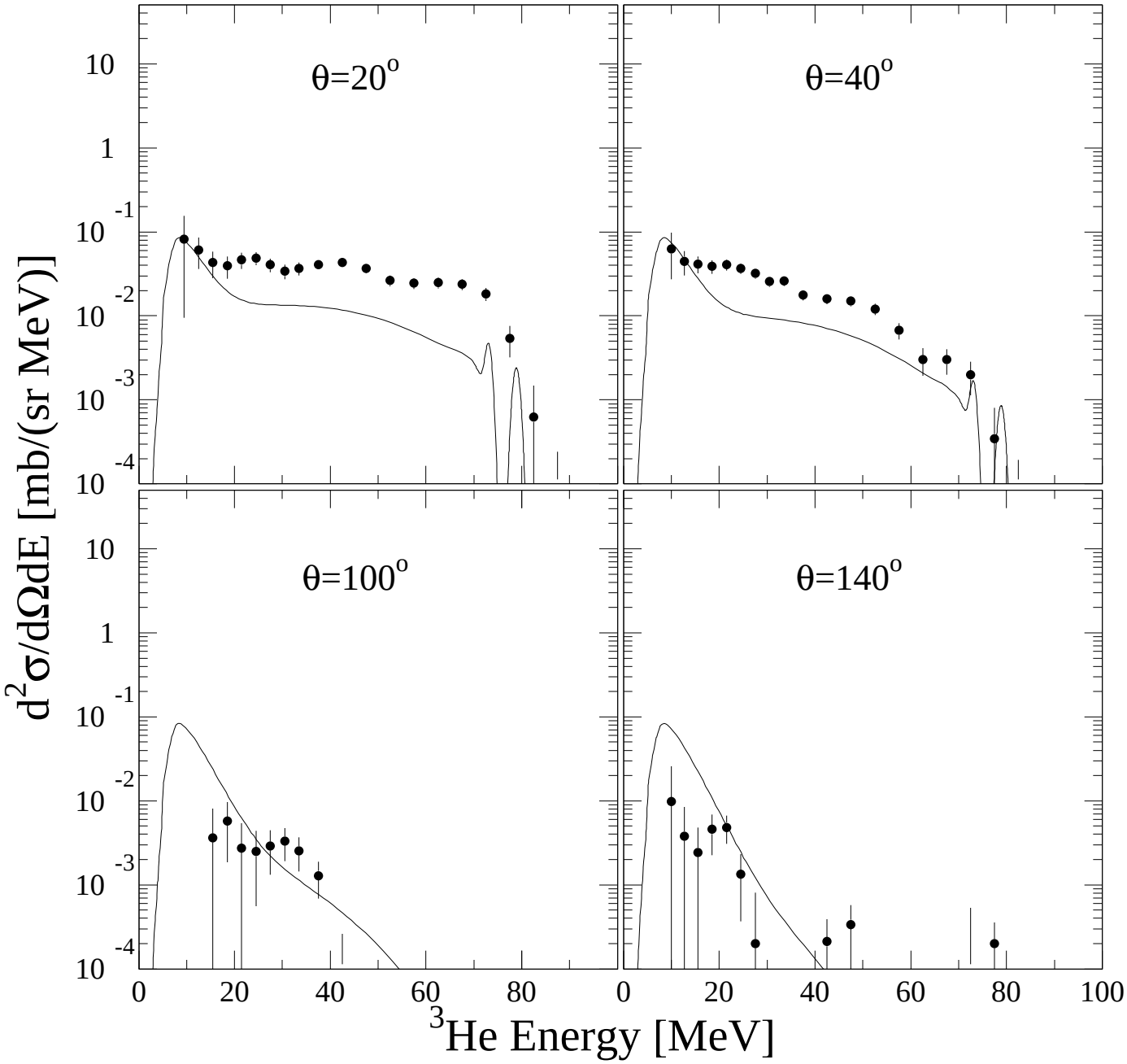
θ=20°
θ=40°
θ=100°
θ=140°
d²σ/dΩdE [mb/(sr MeV)]
³He Energy [MeV]
10
1
10⁻¹
10⁻²
10⁻³
10⁻⁴
0
20
40
60
80
100

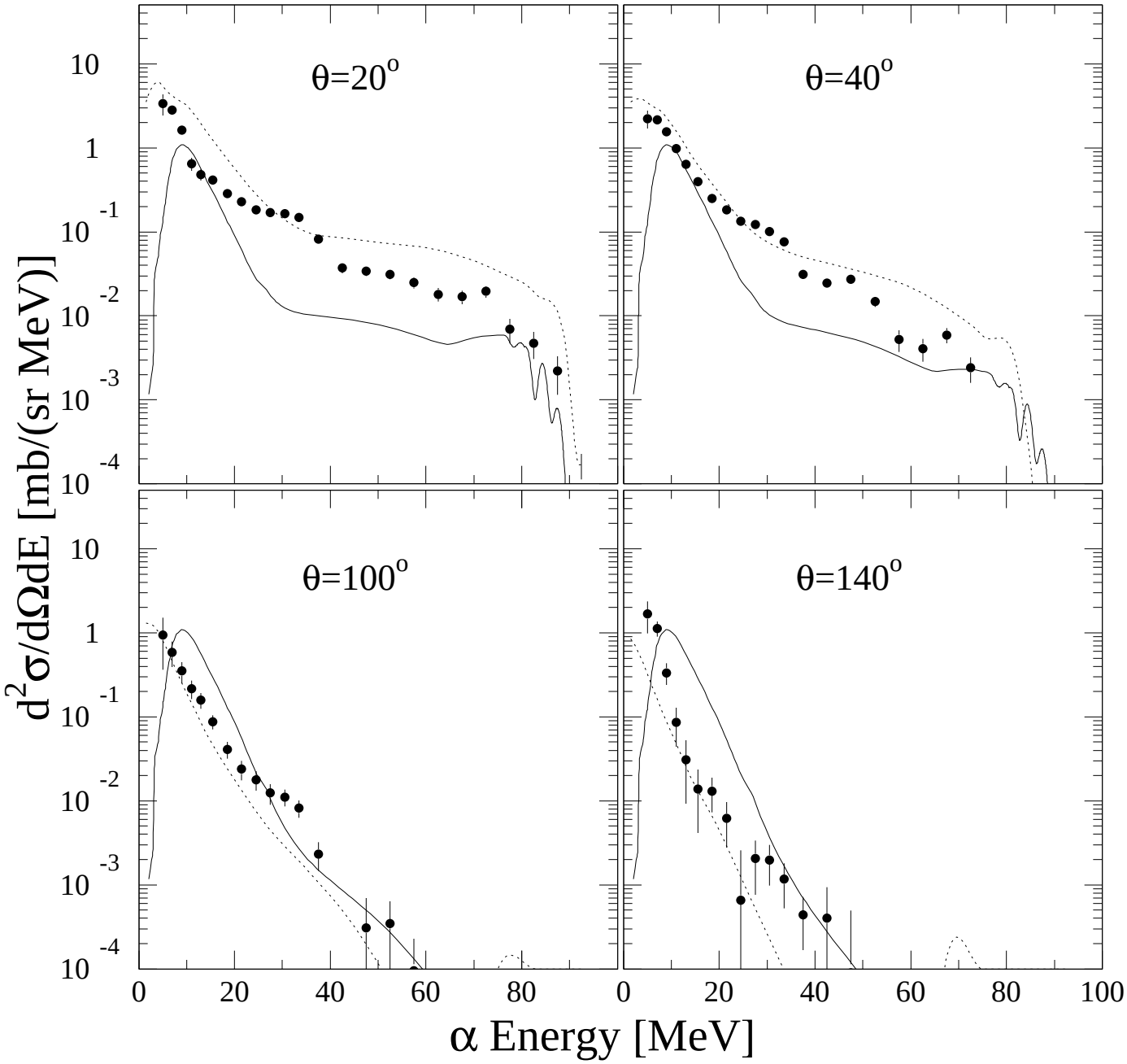
θ=20°
θ=40°
θ=100°
θ=140°
d²σ/dΩdE [mb/(sr MeV)]
α Energy [MeV]
10
1
10⁻¹
10⁻²
10⁻³
10⁻⁴
0
20
40
60
80
100

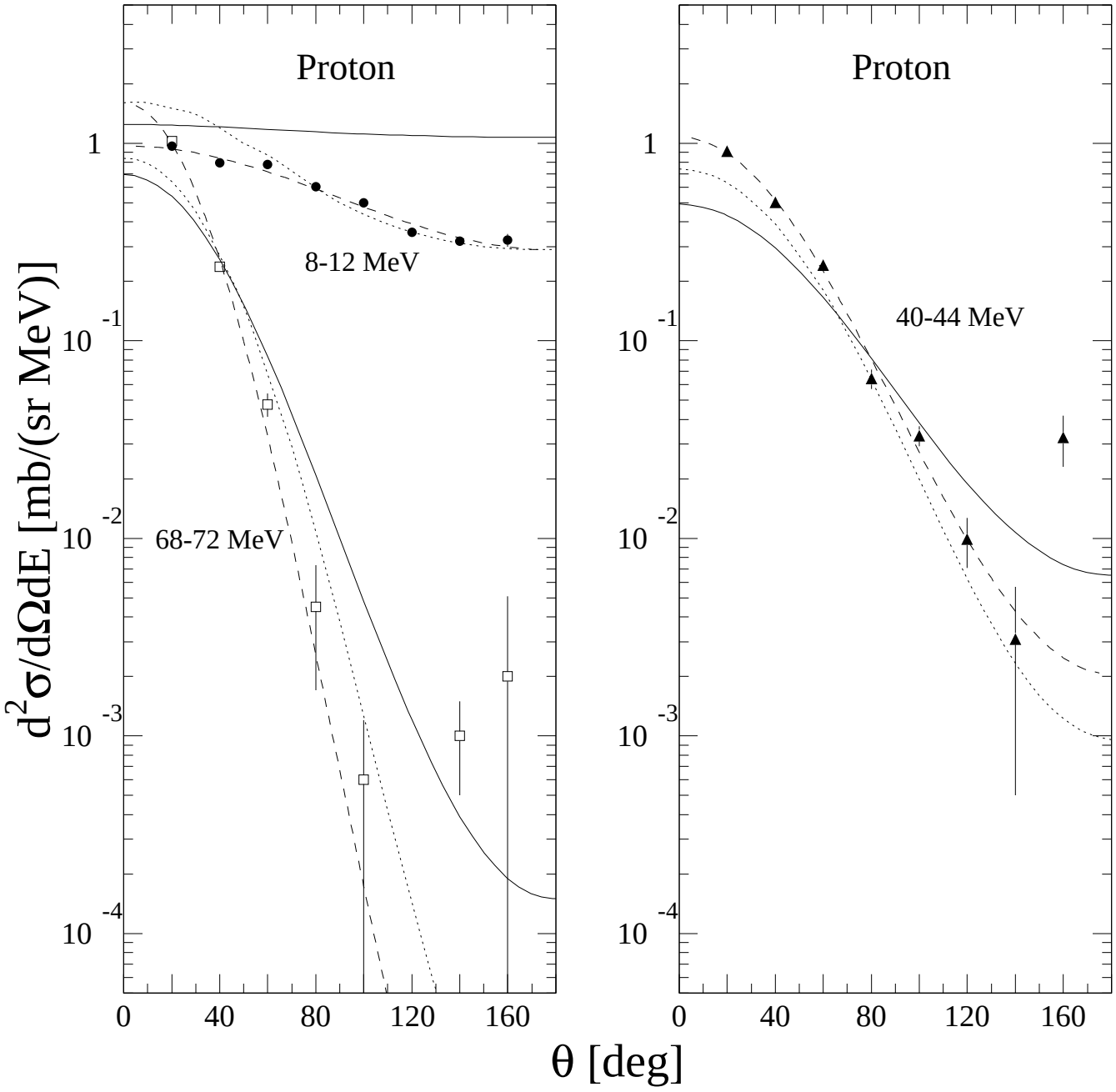
Proton
Proton
8-12 MeV
68-72 MeV
40-44 MeV
d²σ/dΩdE [mb/(sr MeV)]
θ [deg]
1
10⁻¹
10⁻²
10⁻³
10⁻⁴
0
40
80
120
160

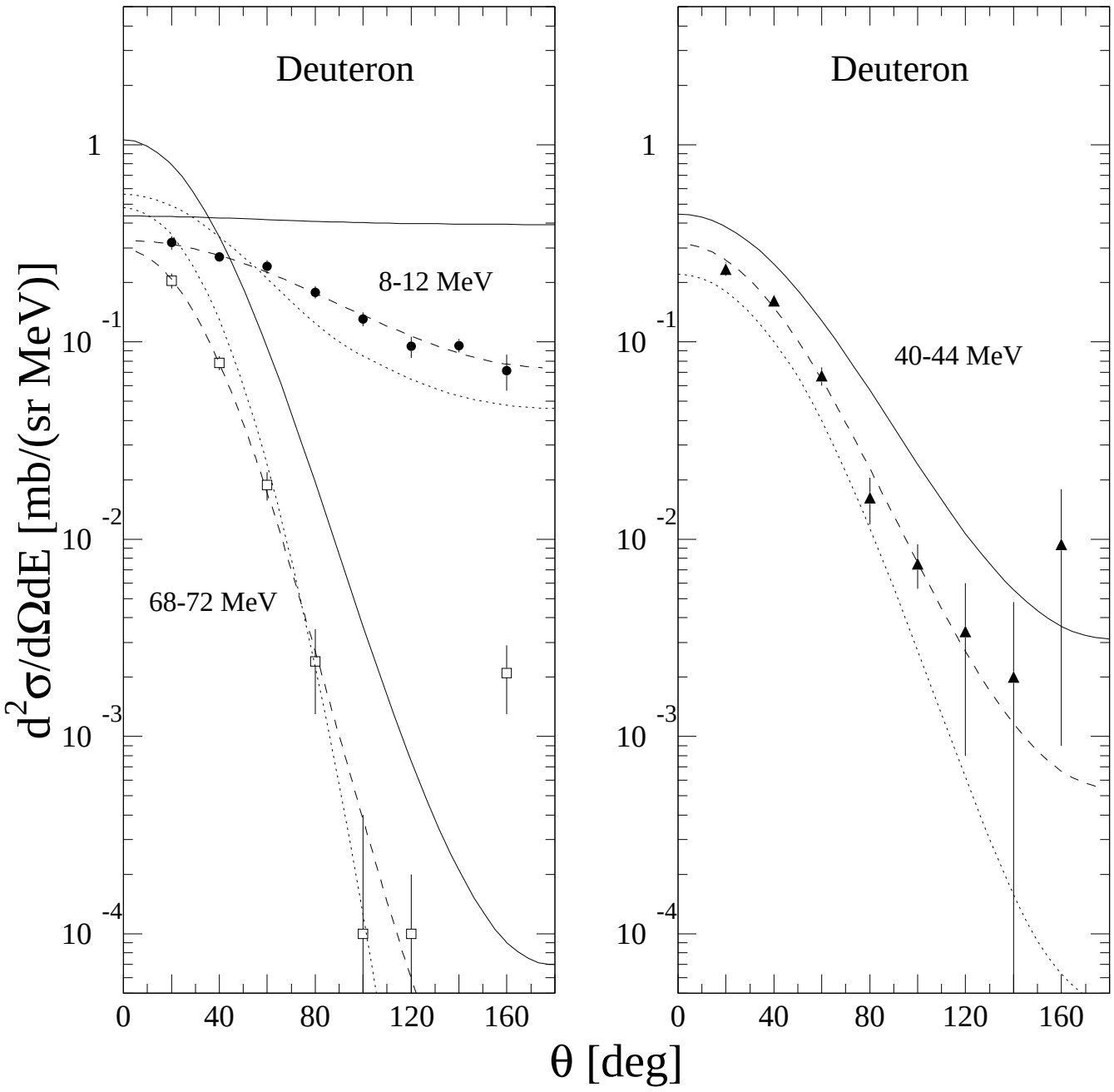
Deuteron
Deuteron
8-12 MeV
68-72 MeV
40-44 MeV
d²σ/dΩdE [mb/(sr MeV)]
θ [deg]
1
10⁻¹
10⁻²
10⁻³
10⁻⁴
0
40
80
120
160

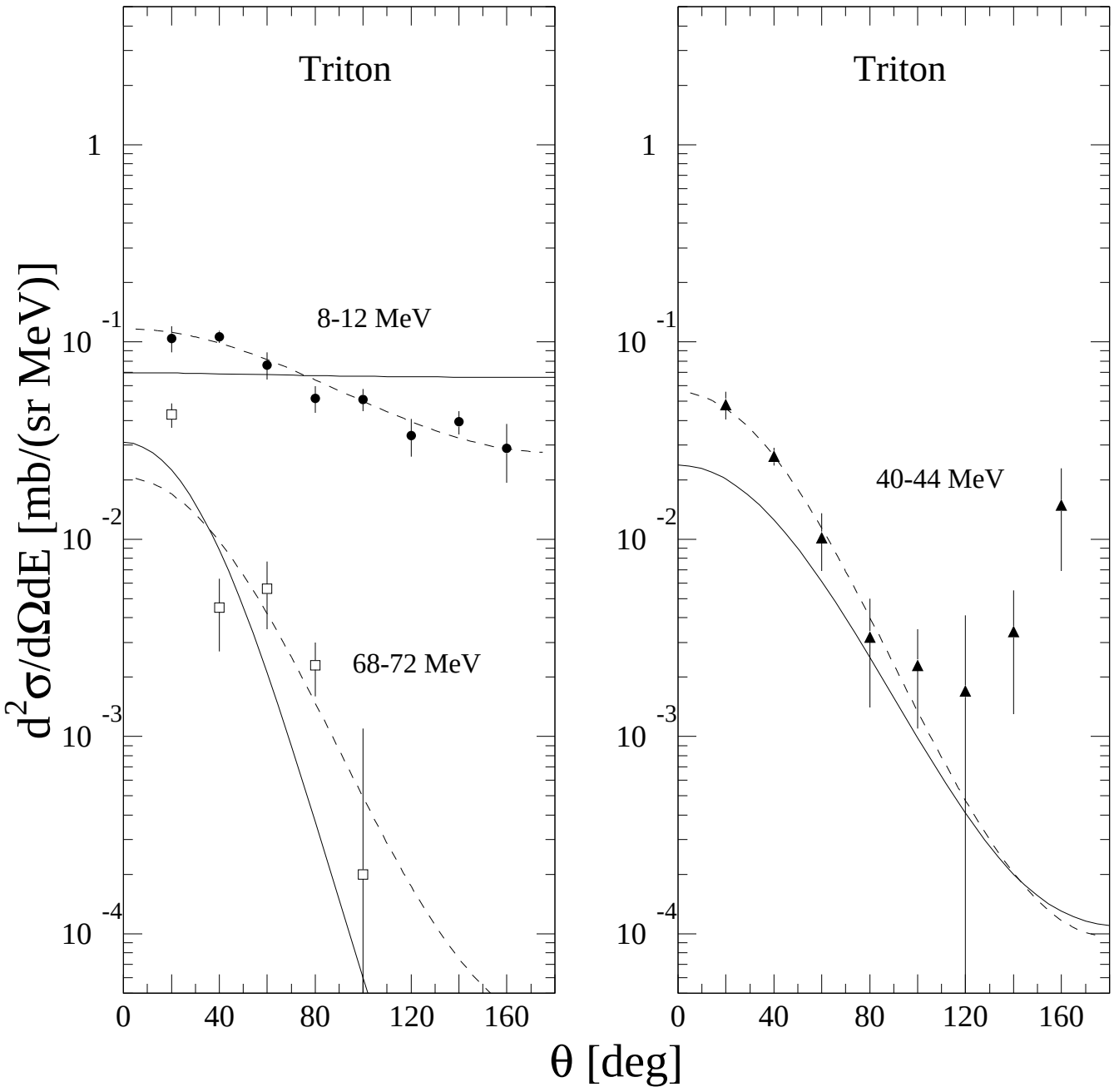
Triton
Triton
8-12 MeV
68-72 MeV
40-44 MeV
$d^2\sigma/d\Omega dE$ [mb/(sr MeV)]
θ [deg]
1
10^{-1}
10^{-2}
10^{-3}
10^{-4}
0
40
80
120
160

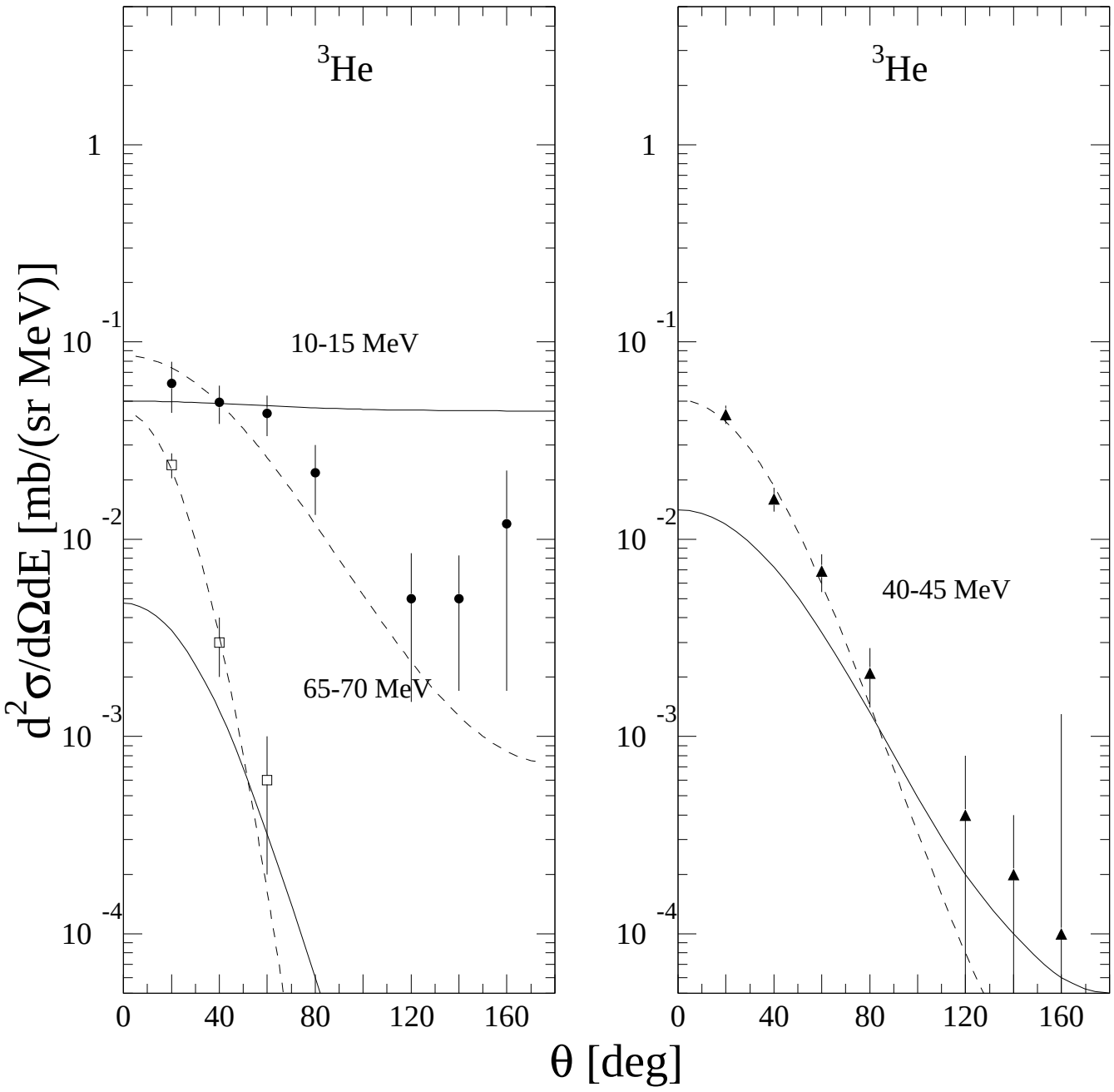
^{3}He
^{3}He
10-15 MeV
65-70 MeV
40-45 MeV
$d^2\sigma/d\Omega dE$ [mb/(sr MeV)]
θ [deg]
1
10^{-1}
10^{-2}
10^{-3}
10^{-4}
0
40
80
120
160

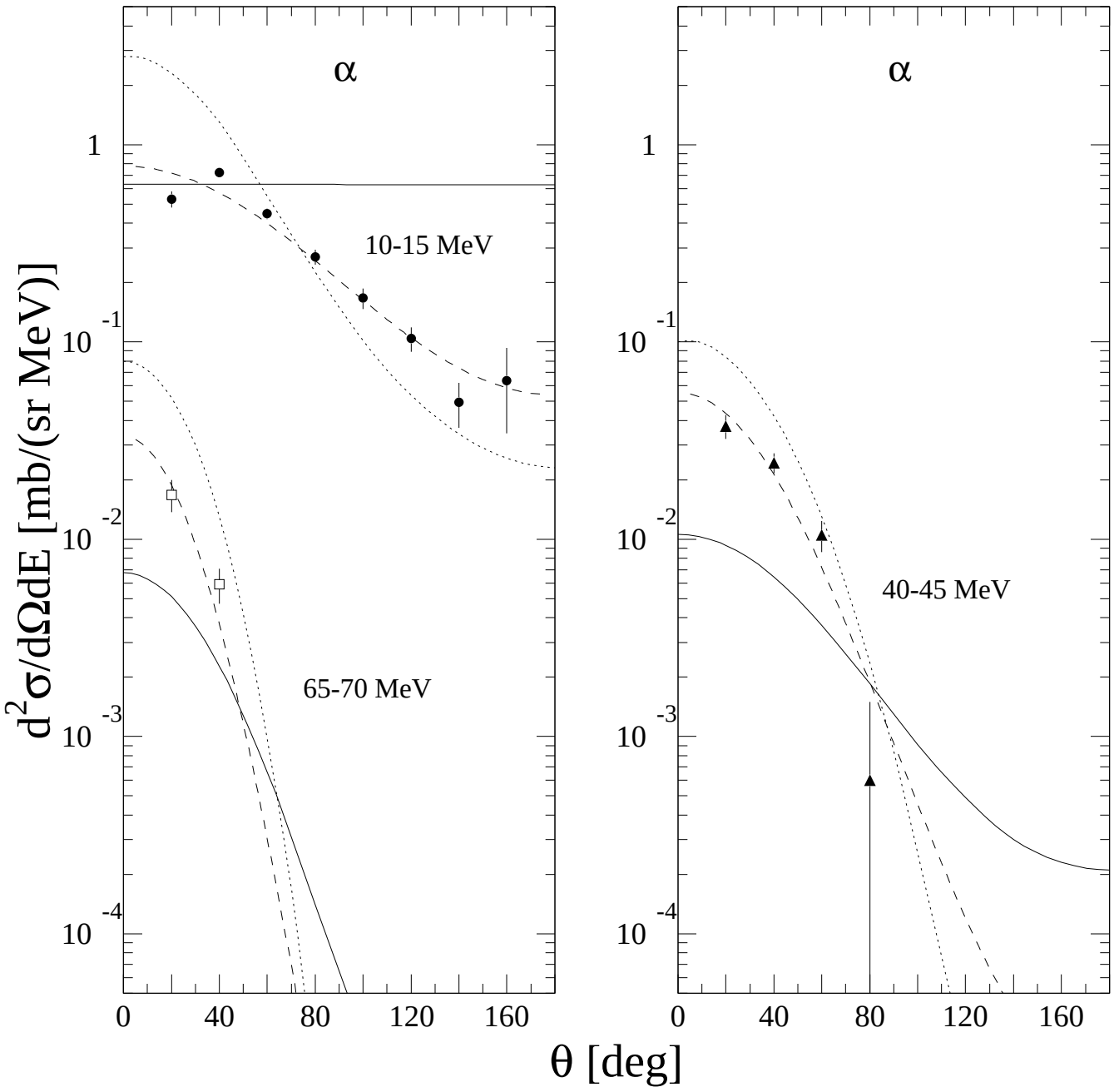
α
α
10-15 MeV
65-70 MeV
40-45 MeV
1
10^-1
10^-2
10^-3
10^-4
0
40
80
120
160
d²σ/dΩdE [mb/(sr MeV)]
θ [deg]

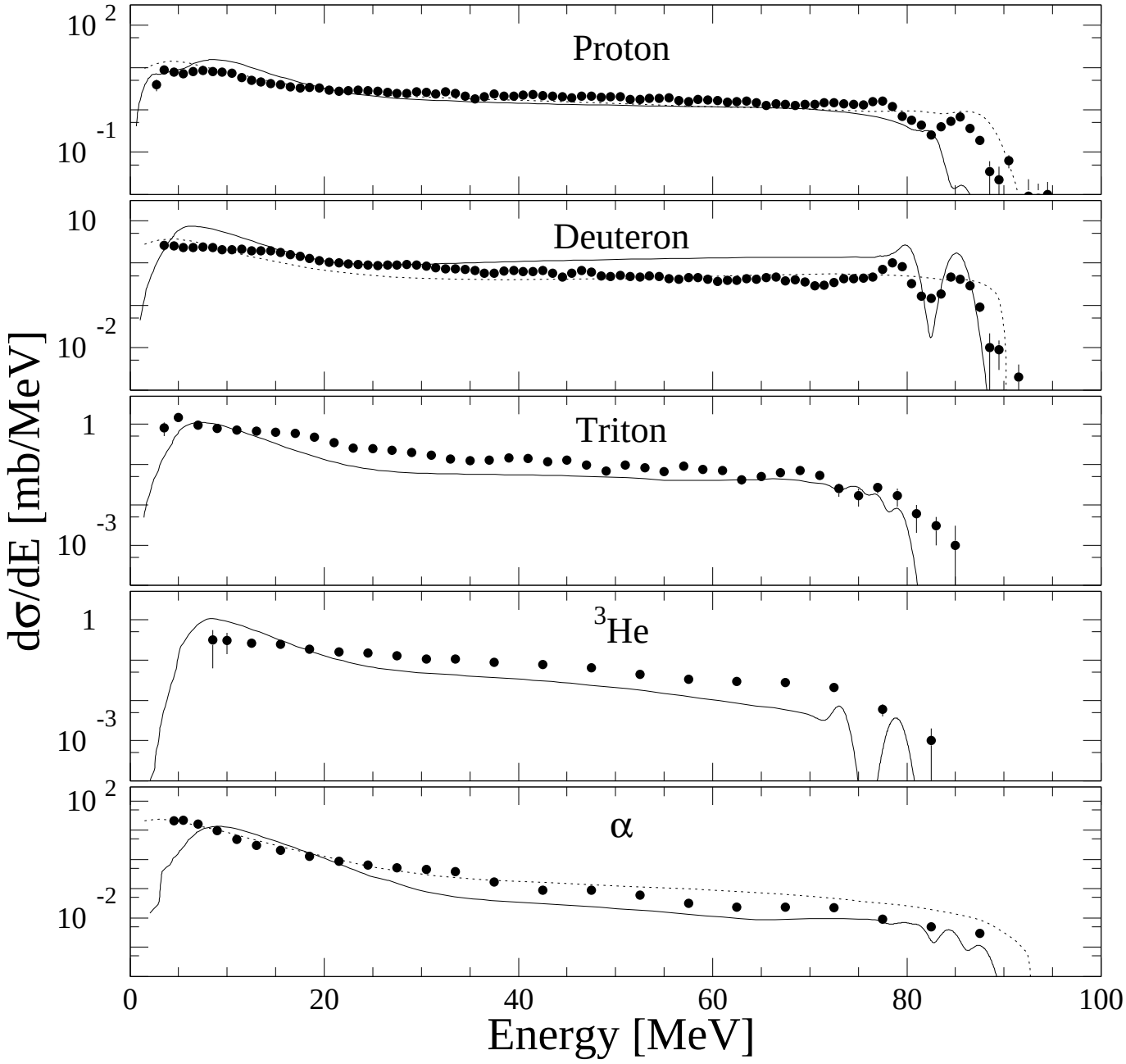
Proton
Deuteron
Triton
^{3}He
α
dσ/dE [mb/MeV]
Energy [MeV]
0
20
40
60
80
100

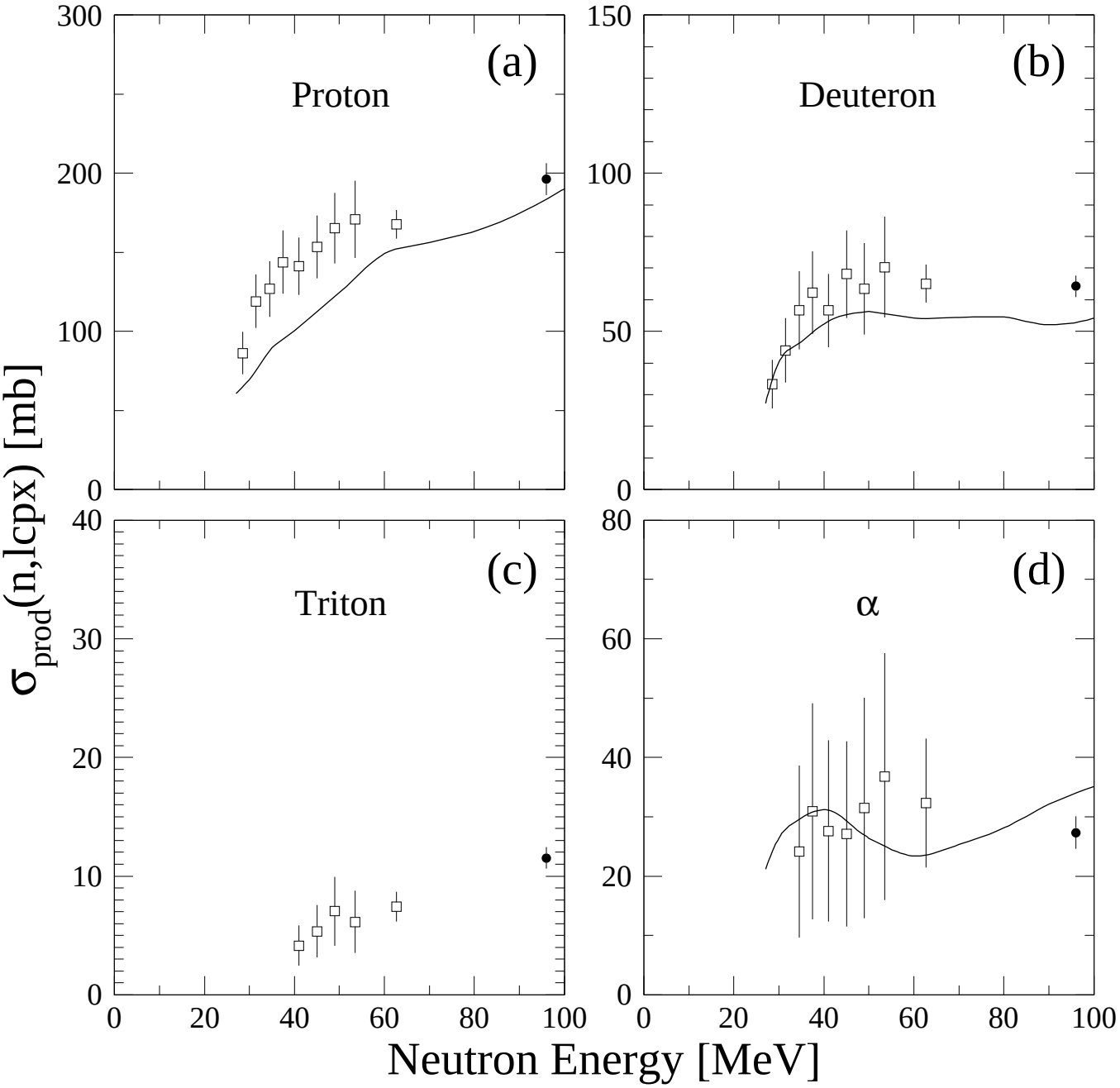
(a)
Proton
(b)
Deuteron
(c)
Triton
(d)
α
σprod(n,lcpx) [mb]
Neutron Energy [MeV]
0
100
200
300
50
150
10
20
30
40
60
80